Development of a Dual Axis Solar Tracking System for Optimizing Sunlight Absorption by Solar Panels Based on IoT

adlian jefiza[1 *] Endriyani1[2*]

[1]Mechatronics Engineering Technology Study Program, Electrical Engineering Department, Politeknik Negeri Batam, Batam, Indonesia

[*]Email: adlianjefiza@polibatam.ac.id, [1 *] meyindriyani02@gmail.com[2*]

Received on dd-mm-yyyy | *Revised on dd-mm-yyyy* | *Accepted on dd-mm-yyyy*

***Abstract*— Solar energy is a promising renewable source with significant potential to reduce dependence on fossil fuels. However, most existing solar tracking systems rely on single-axis tracking, which limits their ability to accurately follow the sun's movement. This research designs a dual-axis solar tracking system that optimizes sunlight absorption by moving the solar panel along horizontal and vertical axes to precisely track the sun's position. The system uses Light Dependent Resistor (LDR) sensors to detect sunlight intensity, DC motors to drive panel movement, and an ESP32 microcontroller as the main control unit, integrated with Wi-Fi for real-time monitoring and control via the Blynk IoT platform. Testing over a full day shows that the dual-axis tracker increased daily energy accumulation efficiency by 38.8% compared to a static panel and by 12.0% compared to a single-axis system. The IoT integration also enables convenient remote monitoring and maintenance, supporting more efficient and sustainable utilization.**

Keywords: Dual Axis, Internet of Things (IoT), Solar Panels, Solar Tracking, Sunlight Optimization

I. INTRODUCTION

Solar energy is a promising and environmentally friendly renewable energy source, especially in tropical countries such as Indonesia that receive high sunlight intensity throughout the year. However, the utilization of this energy remains suboptimal when solar panels are installed statically, because the angle of incidence of sunlight changes dynamically on both a daily and seasonal scale[1]**.** The sun's apparent motion occurs in two main domains, the horizontal domain (azimuth) and the vertical domain (elevation), and its position also shifts monthly due to changes in declination, so that the maximum height and direction of the sun differ between months. These changes cause static panels to be unable to maintain the correct capture angle, so that energy absorption decreases.[2]

Studies show that conventional static solar panels are only able to optimally absorb around 60–70% of solar radiation, mainly because the angle of incidence of light changes throughout the day . When the panel position does not follow the direction of incoming sunlight, the output power decreases significantly, especially in the morning and evening.[3] Solar tracking is therefore an important solution for increasing energy-absorption efficiency. A single-axis system can only follow one of the two domains of solar motion, generally the east–west movement, so the panel cannot fully face the optimal sunlight position, causing significant energy loss, especially due to daily elevation changes and month-to-month shifts in the sun's position.[4] A dual-axis system, in contrast, can follow both domains of solar motion simultaneously, allowing the panel to maintain an orientation that is always perpendicular to the direction of the light, which is the main reason a dual-axis mechanism is more relevant than a single-axis one.[5]

In addition, shows that the absence of an Internet of Things (IoT)-based monitoring system makes it difficult for users to monitor panel performance in real time, so that disturbances or decreases in power are often not detected quickly. This motivates the development of an IoT-based dual-axis solar tracking system that can automatically follow the sun's position throughout the day and provide performance data directly to the user, thereby increasing energy efficiency and enabling more responsive monitoring and maintenance.[6]

Research on solar tracking systems has been carried out using various approaches. A dual-axis solar tracker using Fuzzy Logic Control for the optimization of small-scale photovoltaic power plants (PLTS) has been developed to handle the uncertainty of sunlight intensity so that panel movement becomes smoother and more precise **[7].** Another study developed a dual-axis solar tracker with a water-based actuator combined with a Maximum Power Point Tracking (MPPT) algorithm to optimize electrical energy conversion. Other research used LDR (Light Dependent Resistor) sensors as the main sensor for monitoring dual-axis solar tracker movement, with four LDRs placed at strategic positions to detect differences in light intensity for motor actuation; many other studies used an Arduino Mega 2560 microcontroller as the main processing unit because of its larger number of I/O pins for greater system stability[8]. Meanwhile, other researchers developed automatic solar tracking systems for solar panel charging based on IoT, allowing users to monitor battery-charging status and panel position in real time through an application or web platform, and such tracking systems have been proposed for larger-capacity PLTS installations, where dual-axis tracking is crucial to maximize daily power output compared to permanently installed (static) solar panels [9]. Overall, previous studies show that dual-axis systems provide significantly better results in increasing PLTS efficiency compared to single-axis or static systems, although most studies still focus on either tracking accuracy or the use of standard components rather than the two combined.[10] Studies show that a single-axis, microcontroller-based solar tracker was able to increase output power by 15% compared to a static system [11], while a dual-axis system shows a further increase in efficiency, although still not integrated with a remote monitoring system.[12]

Based on the problems and literature review above, this research designs and builds an IoT-based dual-axis solar tracking system that can optimize sunlight absorption by a solar panel using LDR light sensors to detect the direction of highest light intensity, combined with two DC motor actuators to move the panel horizontally and vertically (dual axis), and integrated with an IoT platform through an ESP32 module so that operational data such as voltage, current, and light intensity can be transmitted and monitored in real time.[13] Specifically, the objectives of this research are: (1) to design a dual-axis solar tracking mechanism that can optimally follow the sun's movement throughout the day; (2) to integrate IoT technology into the system to enable remote monitoring and control through the internet; and (3) to analyze the performance of the resulting IoT-integrated dual-axis solar tracking system.[14] The system is expected to allow users to monitor and control the system in real time from any location, help owners of houses or commercial buildings obtain more solar energy without adding more panels, and make it easier for technicians to periodically monitor performance so that potential damage or efficiency loss can be detected earlier. This research is limited to the design of a small-scale dual-axis solar tracking prototype, does not cover motor or power-supply sizing calculations, limits IoT use to remote monitoring and control, does not analyze the economic aspects of the system, and was tested outdoors under the assumption of clear-weather conditions.[15]

II. METHOD

The stages in the design and development of this IoT-based dual-axis solar tracking system consist of several steps, as shown in Fig. 1.

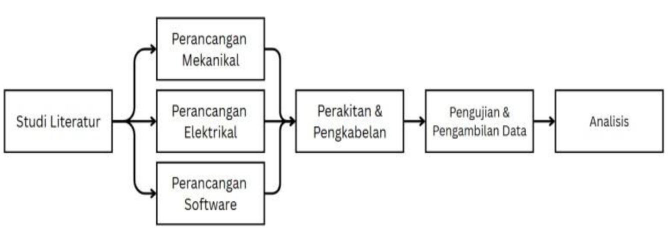

Fig. 1. Research methodology flowchart.

This research began with a literature study to strengthen the theoretical and practical basis, followed by system design covering the mechanical, electrical, and software aspects as a whole. After the final design was completed, fabrication and assembly were carried out, followed by periodic testing to verify that the tool worked as expected; if problems were found, the researcher returned to the design stage for improvement. If the testing was successful, the researcher proceeded to the data collection and analysis stage, where the results were evaluated and discussed; repeated testing or design adjustment could be carried out if needed. The process was considered complete once the tool had been well tested and all data had been comprehensively analyzed.

A. System Block Diagram

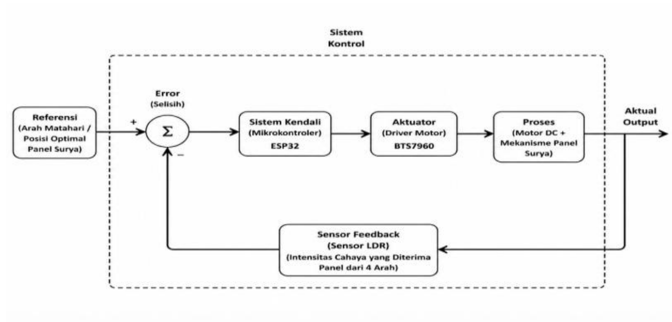

Fig. 2. System block diagram

This dual-axis solar tracker system works by collecting environmental condition data through four LDR (Light Dependent Resistor) sensors and an IMU (Inertial Measurement Unit) sensor as the main inputs. The LDRs detect differences in sunlight intensity, while the IMU provides precise panel-orientation data. An INA3221 sensor directly monitors the solar panel's output power, and four limit switches are installed as a safety feature to limit the physical range of motion of the panel on the horizontal and vertical axes. All input data are processed by the control system through the ESP32 microcontroller. The tracking process begins from a reference value (sun direction/optimal panel position), which is compared with the feedback value from the LDR sensors that detect the light intensity received by the panel from four directions in real time. The difference between the reference and the LDR reading is calculated as an error signal, which is passed to the control system to be converted into a correction command sent to the actuator to rotate the solar panel. The resulting actual output, i.e., the actual change in panel angle/position, is continuously monitored by the LDR sensors as feedback to minimize the error toward zero, so that the panel always faces perpendicular to the sun.

B. System Flow Diagram

The two-axis solar tracker is designed to automatically position the solar panel so that it always faces the sun, both horizontally (azimuth) and vertically (altitude), to maximize sunlight absorption throughout the day. LDR light sensors are placed at various angles around the solar panel; when the sun's position changes, the light intensity received by each LDR differs, and the sensor receiving the brightest light indicates the current sun position. The sensor signal is forwarded to the microcontroller, which determines the required direction of movement and sends commands to the horizontal- and vertical-axis drive motors until the panel is aligned with the direction of the incoming sunlight; the system is also equipped with feedback sensing to ensure the panel is actually positioned as intended.

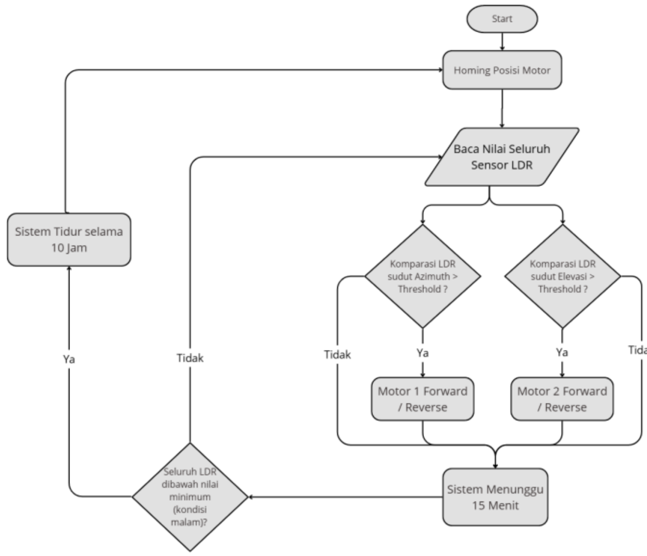

Fig. 3. Program flowchart.

C. Hardware Design

1) Mechanical Design

Fig. 4. Mechanical design of the dual-axis mechanism.

The system is designed to dynamically move the solar panel on two axes of motion: the azimuth (horizontal) axis and the elevation (vertical) axis. The first motor rotates the panel horizontally, following the sun's daily movement from east in the morning to west in the evening, ensuring the panel always faces the sun directly and maximizes sunlight exposure. The second motor adjusts the panel's tilt angle (elevation) to accommodate the change in the sun's height throughout the day and seasons: in the morning and evening the sun is low, so the panel is tilted more steeply, while at midday the sun is at its highest point, so the panel angle becomes shallower. Both motors are driven by the ESP32 microcontroller, which processes light-sensor data to calculate the sun's position in real time.

2) Electrical Design

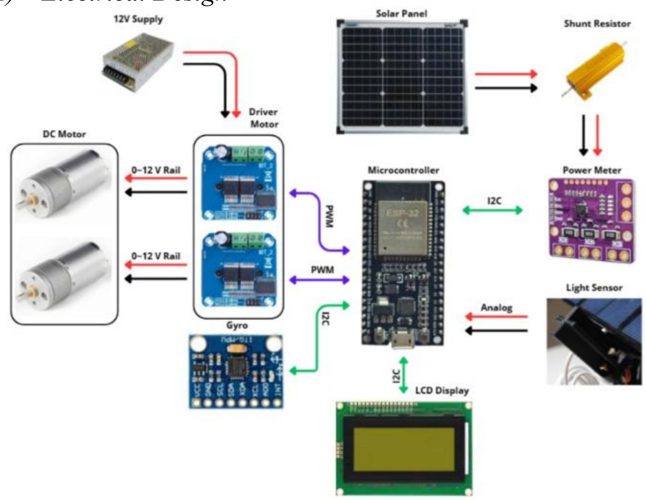

Fig. 5. Electrical system design.

The electrical design supports the performance of the IoT-based two-axis solar tracking system efficiently and stably. The system consists of a solar panel as the main power source, a microcontroller as the control unit, an LDR light sensor to detect the direction of incoming sunlight, and two DC motors to move the panel on the horizontal and vertical axes. An ESP32 connectivity module is used for integration with the internet for remote monitoring and control, and the circuit is equipped with a motor driver to amplify the control signal to the actuators and a power-supply system that regulates voltage distribution to all components.

3) Electronic Design

Fig. 6 and Fig. 7 show the circuit design and PCB layout that serve as the expansion board for the ESP32 module. This board controls the actuators, reads sensor data, houses a step-down converter module to supply optimal power to the ESP32, and includes several LED indicators to support the system design process.

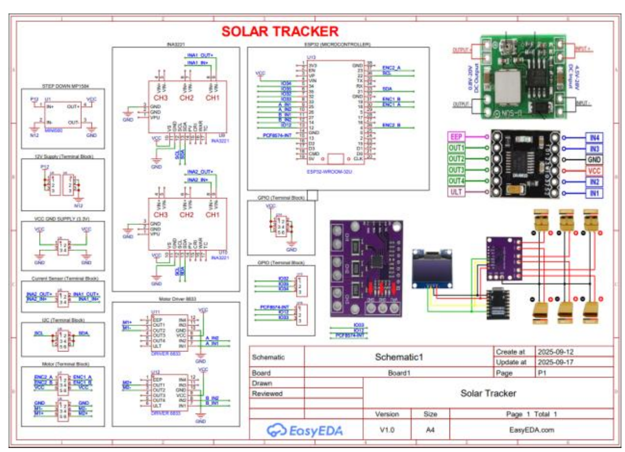

Fig. 6. Circuit design of the expansion board (PCB).

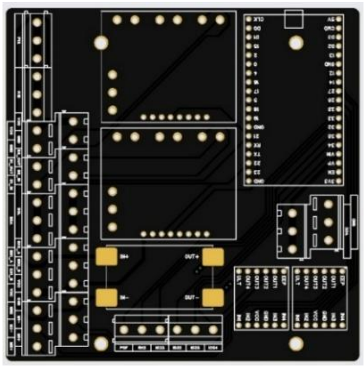

Fig. 7. Expansion board for the microcontroller.

4) Dummy Load Design

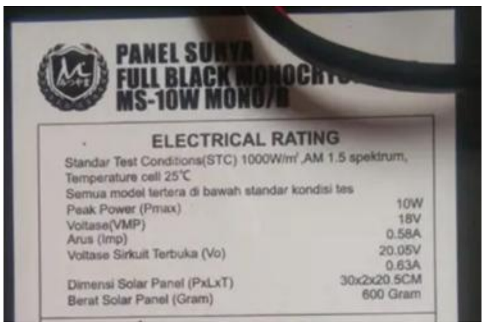

Fig. 8. Solar panel electrical specifications.

A dummy load is used so that the solar panel has a working load during testing, because without a load the panel only produces open-circuit voltage and the measured current does not represent real conditions; with a dummy load the panel can carry current so that voltage, current, power, and efficiency can be measured more accurately, while also simulating real working conditions without requiring a battery or other electronic device, making testing simpler, safer, and more stable.

The relationship between voltage, current, and resistance follows Ohm's law. With a panel specification of a maximum voltage of 18 V and a maximum current of 0.58 A, the theoretical load resistance is:

$$R = 18 / 0.58\ \Omega = 31\ \Omega \quad (1)$$

The nearest standard resistor value is 30 Ω, so the resistor can draw current nearly to the panel's maximum. The power dissipated by the resistor is:

$$P = 18^2 / 30 = 10.8\ \text{W} \quad (2)$$

Based on this calculation, a 30 Ω, 25 W shunt-resistor dummy load is suitable for a 10 Wp, 18 V, 0.58 A solar panel because it can produce a working current of about 0.6 A, close to the panel's maximum current. The resistor's power dissipation of about ±10.8 W is well below its 25 W maximum capacity, so it can operate safely, stably, and without overheating during testing.

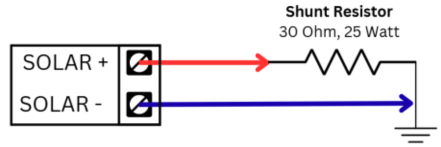

Fig. 9. Solar panel dummy load circuit.

The positive terminal of the solar panel is connected to the resistor through a red wire, while the negative terminal is connected directly to ground through a blue wire, forming a closed circuit; the resistor acts as an artificial load to absorb power from the panel so that its voltage and current can be tested under real working conditions.

D. Software Design

1) Control System

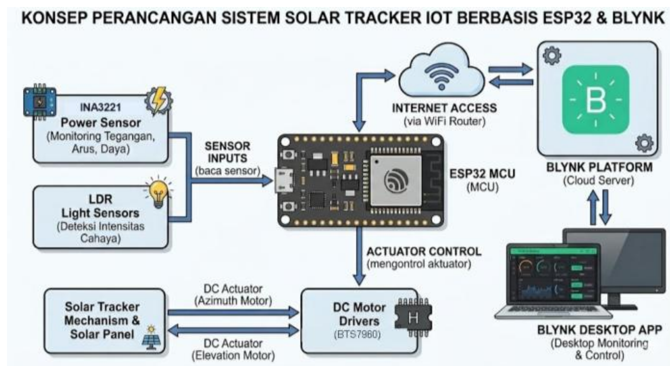

Fig. 10. System software architecture.

The software aims to automatically regulate the system's working logic and enable remote monitoring and control. The main logic includes reading light-sensor (LDR) data, comparing the light intensity from four directions, and commanding DC motor movement to adjust the panel's position so that it always faces the direction with the highest light intensity. The software also handles data communication over Wi-Fi, enabling integration with the Blynk IoT platform for monitoring temperature, panel position status, and manual control from the application, and is equipped with auto-calibration and data-logging features to facilitate analysis of panel performance over time.

2) Blynk IoT Dashboard

Fig. 11. Blynk IoT dashboard.

The dashboard, built on the Blynk IoT platform, serves as the wireless control and monitoring center between the user and the ESP32 hardware installed in the field. It is divided into two main functions: manual control and real-time electrical-parameter monitoring. At the top of the dashboard there are a Manual Control button and navigation controls for Motor 1 and Motor 2 (Forward, Reverse, Stop) that allow the user to move the panel position manually via smartphone or computer, as well as an axis-angle indicator that displays the panel's tilt position on both axes. The dashboard also has a data-logging feature visualized as graphs and numeric widgets, monitoring voltage (V), current (mA), and power (W), along with trough and peak statistics for each parameter, and a Super Chart showing the data trend over time to help the user analyze fluctuations in sunlight absorption throughout the day.

E. Supporting Component

The system uses an ESP32 System-on-Chip microcontroller with built-in Wi-Fi/Bluetooth connectivity and a dual-core 32-bit processor running up to 240 MHz, power-saving modes such as deep sleep, and multiple GPIO pins for digital I/O, PWM, and external-device communication, programmable through the Arduino IDE, ESP-IDF, or Platform IO. DC motors, comprising a stator, rotor (armature), commutator, brushes, and shaft, act as the horizontal- and vertical-axis actuators, driven through BTS7960 motor drivers that bridge the microcontroller and the motors, allowing direction (CW/CCW) and speed control on both axes through the H-Bridge principle, since the ESP32 cannot directly supply sufficient current to the motors. A 16×4 LCD with an I2C module serves as a local monitoring interface, displaying LDR readings, panel tilt angle, and the panel's voltage and current values. Four limit switches, mounted at the maximum rotation limits of the elevation and azimuth axes, act as a mechanical safety device, sending a signal to the ESP32 to automatically stop the motor when triggered, preventing cable twisting or mechanical damage from over-rotation. Four LDR sensors, whose resistance decreases as incident light becomes brighter, are used to detect the direction of the sun. An INA3221 high-precision sensor module, working through a shunt resistor and I2C communication, measures the panel's output voltage, current, and power for efficiency comparison between the static and tracked panel. A switching power supply provides stable electrical energy to all components, and a DC step-down (buck converter) module lowers the 12 V source voltage to the 5 V or 3.3 V required to safely supply the ESP32, sensors, and LCD. An MPU6050 Inertial Measurement Unit (IMU), combining a 3-axis accelerometer and a 3-axis gyroscope and communicating through I2C, is mounted on the back of the solar panel to read the actual panel tilt angle relative to the horizontal plane in real time. Although the sensor physically detects motion on 6 axes, the tracker control system extracts only the pitch angle, which is mapped to represent the panel's elevation angle, as illustrated in Fig. 12. Finally, the Blynk IoT platform, consisting of the Blynk App, Blynk Server, and Blynk Libraries, serves as the wireless control and monitoring hub, receiving LDR readings and panel voltage status sent by the ESP32 to the Blynk Cloud for real-time display on a smartphone application and allowing manual remote intervention to move the DC motors when needed.

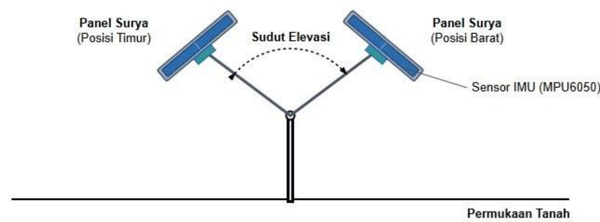

Fig. 12. Illustration of panel movement at the elevation angle.

III. RESULT AND DISCUSSION

A. Assembly Result

1) Mechanical

Fig. 13. Mechanical assembly result.

The mechanical assembly consists of several integrated components: a panel box that protects the electronic circuit from weather, dust, and external interference while housing the system controls; a base plate that serves as the main foundation, providing structural stability and a mount for the motion mechanism and solar panel; a two-axis motion mechanism that allows the panel to move on the azimuth and elevation axes so that it can optimally follow the direction of sunlight intensity throughout the day; the solar panel, mounted on top of the two-axis mechanism, as the main element converting light energy into electrical energy; and a four-point LDR sensor mounted at strategic positions to detect light intensity from various directions as a reference for accurately driving the tracking system. Overall, the assembly shows that all mechanical components are well integrated, enabling the solar tracker system to work responsively in following the sun's movement to maximize energy-absorption efficiency.

2) Electrical

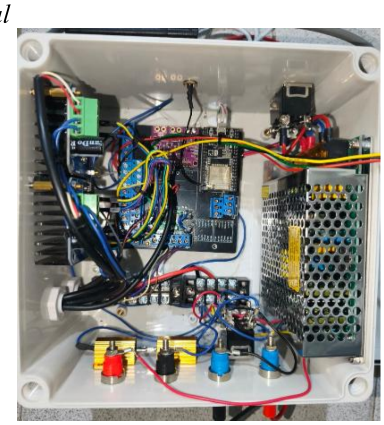

Fig. 14. Electrical assembly inside the panel box.

The electrical assembly consists of a power supply and a PCB board as the main control center. The power supply provides the voltage that supplies the whole system, while the PCB board integrates the ESP32, a 5 V step-down converter, a current sensor, and a terminal block. The ESP32 acts as the main microcontroller that processes sensor data and controls the system, the step-down converter lowers the voltage to the appropriate level, the current sensor monitors the system's current consumption, and the terminal block is used for neat and safe inter-component connections. Two BTS7960 motor drivers are connected to the actuator motors for precise panel movement, power distribution is supported by an industrial switching power supply (SMPS) to ensure stable voltage to all components, and the wiring is arranged using terminal blocks and cable ties, showing a systematic integration between the high-voltage (AC) power lines and the low-voltage (DC) signal lines.

B. Component Testing

1) ESP32-to-Blynk Response

Testing of the ESP32-to-Blynk dashboard response was carried out in 10 consecutive trials to evaluate the reliability of the device's wireless communication, as recorded in Table I.

TABLE I. RESPONSE OF THE ESP32 SYSTEM TO THE BLYNK SERVER

Trial No.	Time	Connection Status	Server Response (ms/sec)	Data Transmission
1	13/07/2026 [20:25]	Connected	8	Success
2	14/07/2026 [06:10]	Connected	7	Success
3	14/07/2026 [19:20]	Connected	9	Success
4	15/07/2026 [05:52]	Connected	6	Success
5	15/07/2026 [21:02]	Connected	8	Success
6	16/07/2026 [06:13]	Connected	7	Success
7	16/07/2026 [18:56]	Connected	10	Success
8	16/07/2026 [19:51]	Connected	9	Success
9	17/07/2026 [05:00]	Connected	8	Success
10	17/07/2026 [06:10]	Connected	7	Success
Rata-rata			7.9	Success [100%]

The results show very optimal performance with an average data-transmission success rate of 100%, with all trials successful, proving that the integration between the ESP32 hardware and the Blynk platform has very good data-transmission stability without any packet loss, making it reliable for supporting the system in real time.

2) ESP32 Delay Latency

Delay/latency testing measures the time required by the ESP32 to send or receive electrical-parameter data over the internet, a parameter that is crucial in real-time IoT systems such as solar trackers because delayed data transmission can affect the currency of information displayed on the dashboard, as presented in Table II.

Based on the test results, the average delay obtained is within a very safe range for an IoT-scale system, on the order of milliseconds. Although there is slight fluctuation in response time at some data points due to internet bandwidth stability and Wi-Fi signal strength in the test area, overall the data-communication process runs successfully without any packet loss, proving that the ESP32's internet connectivity has reliable performance and can support real-time system-parameter monitoring; the Blynk dashboard's Developer Tools page confirms that the device is consistently Online with stable network response speed.

TABLE II. ESP32 DELAY LATENCY

Trial No.	Time	Connection Status	Server Response (ms/sec))
1	13/07/2026 [20:25]	Connected	139
2	14/07/2026 [06:10]	Connected	156
3	14/07/2026 [19:20]	Connected	165
4	15/07/2026 [05:52]	Connected	156
5	15/07/2026 [05:52]	Connected	186
6	16/07/2026 [21:02]	Connected	140
7	16/07/2026 [18:56]	Connected	120
8	16/07/2026 [19:51]	Connected	155
9	17/07/2026 [05:00]	Connected	159
10	16/07/2026 [06:10]	Connected	175
Rata-rata			155

3) LDR Sensor Testing

LDR sensor testing was carried out by observing the sensor's output values based on actual lighting conditions from morning to evening, to verify that the sensor can accurately detect sunlight intensity and correctly control the direction of panel movement, as shown in Table III.

TABLE III. LDR SENSOR TESTING

Trial No	Time	LDR 1	LDR 2	LDR 3	LDR 4	Remarks
1	6:00	847	790	454	439	Sun begins to rise in the East (dim dawn conditions)
2	7:00	1833	1754	594	576	Morning sunlight becomes dominant on the East side
3	8:00	3245	3348	893	854	Morning sunlight begins to dominate on the East side
4	9:00	3892	3946	1426	1362	Late morning approaching noon; LDR 3 nearing the upper limit
5	10:00	4013	3981	2140	1988	High intensity on the East side approaching midday
6	11:00	4078	4194	3251	3098	Sun position very high; other LDRs begin to rise sharply
7	12:00	4095	4095	4095	4095	Sun directly overhead (highest peak/total saturation)
8	13:00	4031	2169	3422	3319	Sun begins tilting toward the West
9	14:00	1039	819	3419	2284	Midday heat transitioning to afternoon, dominated by the West side
10	15:00	713	805	1632	1498	Afternoon; light intensity begins to decrease gradually
11	16:00	524	573	1025	1231	Sun preparing to set on the Western horizon
12	17:00	455	493	760	851	Afternoon transitioning toward dusk
13	18:00	402	410	557	521	Dusk/sunset ;values return to the lower baseline range

Data acquisition was performed by recording the four LDR sensor readings on the Arduino IDE Serial Monitor in the form of analog (ADC) value strings from each sensor.

4) Actuator Testing

Actuator testing aims to ensure that the solar panel can move correctly, following the direction of the light source based on LDR sensor data, using a DC motor controlled through a motor driver, as recorded in Table IV and illustrated by the motor-movement logic in Fig. 15.

TABLE IV. ACTUATOR TESTING AGAINST THE SENSOR

Trial No.	LDR 1	LDR 2	LDR 3	LDR 4	M1	M2	Remarks
1	3482	3575	2015	1934	Forward	Hold	Light dominant above
2	1540	1612	3245	3618	Reverse	Hold	Light dominant below
3	1985	3764	3692	1910	Hold	Forward	Light dominant on the right

4	3526	1845	1923	3614	Forward	Reverse	Light dominant on the left
5	3912	4025	2035	1994	Forward	Forward	Light very bright at upper-center
6	3465	3890	3382	1975	Forward	Forward	Light diagonally upper-right
7	2142	3625	3548	2210	Hold	Forward	Horizontal position correction, right
8	3025	3054	2965	3012	Hold	Hold	Balanced condition
9	532	548	495	512	Hold	Hold	Balanced condition
10	3385	2042	3314	1925	Forward	Reverse	Light diagonally upper-left

Note :

- Threshold_X = 100
- M1 Logic
  - Avg (1+2) – Avg(3+4) > Threshold_X =M1 Forward
  - Avg (3+4) – Avg(1+2) > Threshold_X =M1 Reverse
- M2 Logic
  - Avg (2+3) – Avg(1+4) > Threshold_X =M2 Forward
  - Avg (1+4) – Avg(2+3) > Threshold_X =M2 Reverse

Based on the test data and motor-movement logic, the four-LDR control system proved to work well and accurately: when the sun's position shifted and caused the average ADC value difference between the LDRs to exceed the threshold (100), the microcontroller immediately responded by driving motor M1 or M2 (Forward/Reverse) to reposition the solar panel (Trials 1–7); the system also successfully drove both motors simultaneously when light came from a diagonal direction (Trials 6 and 10), so that the panel always faced perpendicular to the incoming sunlight optimally. The threshold value of 100 proved effective in keeping the motor stable and avoiding unnecessary vibration or continuous movement (hunting), as shown in Trials 8 and 9, where the motor remained stationary (hold) when the LDR value difference was below 100, both in bright and overcast weather; this tolerance limit saves motor power consumption and keeps the gearbox mechanical components from wearing out quickly due to frequent start-stop operation.

5) Solar Panel Output Testing

Solar panel testing aims to determine the panel's performance in producing electrical power based on position, light intensity, and sun-tracking effectiveness. Voltage and current were measured directly using a multimeter, and the power value was calculated using the basic electrical formula:

$$Power\ (W) = Voltage\ (V) \text{ x } Current\ (A) \qquad (3)$$

TABLE V. SOLAR PANEL OUTPUT TESTING

Trial No.	Voltage (V)	Ampere (A)	Watt (W)
1	18.04	241.7	4.36
2	17.98	252.5	4.54
3	17.65	228.1	4.03
4	17.28	182.4	3.15
5	15.45	118.6	1.83
6	11.42	46.2	0.53
7	6.35	5.4	0.03
8	12.24	43.5	0.53
9	15.42	132.8	2.05
10	17.52	200.4	3.51
11	12.61	76	0.96
12	15.42	115.2	1.78

Overall, the test results in Table V show that the solar panel used functions well; fluctuations in the values in each trial confirm the importance of implementing a solar tracker system to keep the panel position following the sun's direction so that the output produced remains optimal.

6) INA3221 Sensor Testing

INA3221 sensor testing was carried out to verify the accuracy of the electrical-parameter readings (voltage, current, power) produced by the solar panel before being processed by the ESP32, by comparing the values read on the 16×4 LCD screen with reference values measured using an external digital multimeter in real time. The sensor is installed in series on the load path to measure current and in parallel to measure input voltage. The comparison data between the INA3221 sensor and the digital multimeter from 06:00 to 18:00 WIB are presented in Table VI.

TABLE VI. COMPARISON OF MEASUREMENTS BETWEEN THE MULTIMETER AND INA3221

Time	Voltage (V)		Ampere (A)		Watt (W)	
	INA3221	**Multimeter**	**INA3221**	**Multimeter**	**INA3221**	**Multimeter**
6:00	12.15	12.00	47.2	45.0	0.57	0.54
7:00	15.98	15.80	134.5	130.0	2.15	02.05
8:00	17.62	17.40	206.8	200.0	3.64	3.48
9:00	18.05	17.80	231.4	225.0	4.18	04.01
10:00	18.28	18.00	246.5	240.0	4.51	4.32
11:00	18.25	18.00	256.3	250.0	4.68	4.50
12:00	18.26	18.00	257.1	250.0	4.69	4.50
13:00	18.14	17.90	252.6	246.0	4.58	4.40
14:00	17.95	17.70	230.2	225.0	4.13	3.98
15:00	17.48	17.20	185.7	180.0	3.25	3.10
16:00	15.55	15.30	124.6	120.0	1.94	1.84
17:00	11.42	11.20	50.8	48.0	0.58	0.54
18:00	6.72	6.50	6.5	5.0	0.04	0.03

Overall, the voltage, current, and power fluctuations from morning to evening show the same trend between the two measuring instruments. To evaluate the accuracy of the INA3221 sensor against the multimeter as the reference instrument, absolute and relative error analysis was used, calculated as:

$$\Delta x = x_0 - x \qquad (4)$$

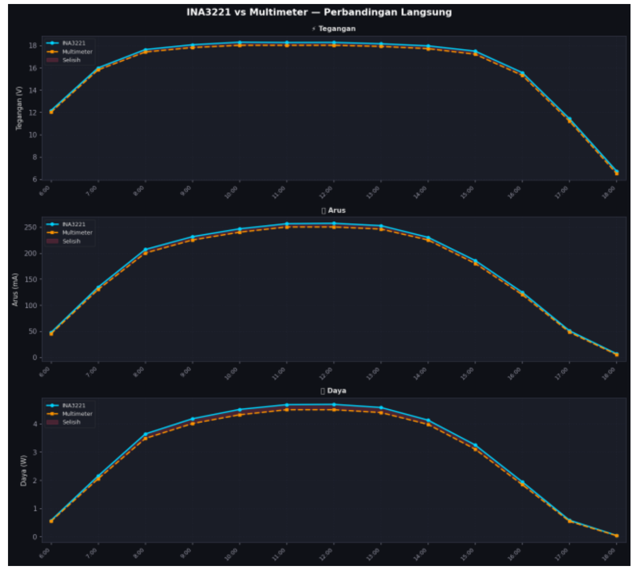

Fig. 16. Visualization of the comparison between the multimeter and INA3221.

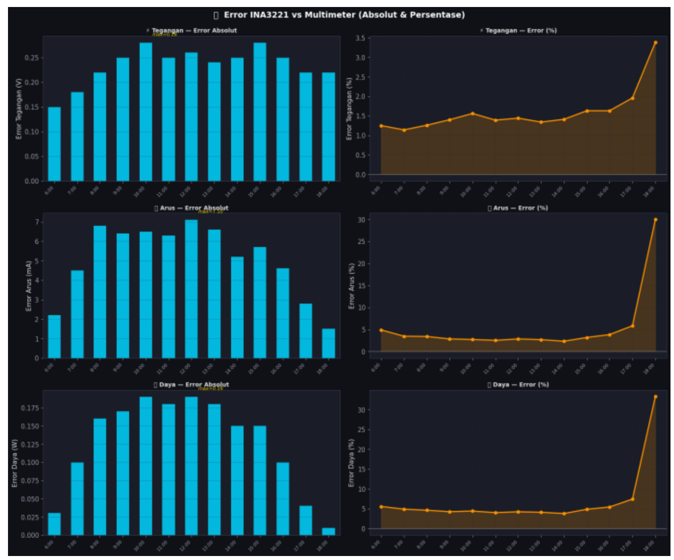

Fig. 17. Visualization of INA3221 error values.

Based on testing from 06:00 to 18:00 WIB, the INA3221 sensor shows a very good ability to follow the trend of voltage, current, and power changes in real time; its reading curve is almost identical to the multimeter's measurement results. However, the INA3221 sensor consistently reads slightly higher (over-read) throughout the measurement period. The largest absolute difference occurred at midday during peak conditions (11:00–12:00), with a maximum power difference ranging between 0.18–0.19 W. This consistently positive difference indicates a systematic offset factor in the sensor rather than random error.

Although the absolute error value increases under midday conditions, the percentage-error graph instead shows the opposite pattern: the largest percentage error occurs in the morning and evening when the voltage and current values are at their lowest, a common characteristic of electronic sensors whose relative accuracy decreases slightly when reading very small values. At peak power at midday, the power-error percentage is only around 3–4%, calculated as:

$$Error\ (\%) = \left|\frac{Value\ Multimeter - Value\ INA3221}{Value\ Multimeter}\right| x\ 100\% \quad (1)$$

TABLE VII. COMPARISON OF MEASUREMENTS BETWEEN THE MULTIMETER AND INA3221

Parameter	Average Absolute	Average Error Percentage (%)
Voltage (V)	0.22 V	1.46%
Current (mA)	4.62 mA	4.92%
Power (W)	0.13 Watt	5.85%

This small error value proves that the INA3221 sensor has high accuracy and is very suitable for use in an energy-monitoring system on a solar tracker.

C. Field Testing

1) Testing Location

Although the physical testing of this dual-axis solar tracker was carried out at geographic coordinates in the city of Batam, the applied tracking control system is designed to be independent of geographic location; the system works dynamically by directly comparing the difference in light-intensity values from the LDR sensors, so that if this system is moved to any location on Earth, it will still be able to detect the direction of incoming sunlight and perform two-axis tracking automatically.

TABLE VIII. SOLAR TRACKER EFFICIENCY TESTING

Time	Voltage		
	Tracker -2 Axis	Tracker -1 Axis	Static
06:00	12.00	9.62	5.50
06:30	13.80	11.75	8.30
07:00	15.80	14.39	11.80
07:30	16.80	15.83	13.00
08:00	17.40	16.99	16.20
08:30	17.80	17.57	17.50
09:00	17.80	17.80	17.90
09:30	17.90	17.90	17.90
10:00	18.20	18.14	18.00
10:30	18.90	18.72	18.50
11:00	18.90	18.90	18.90
11:30	18.90	18.90	18.90
12:00	18.90	18.90	18.90
12:30	18.90	18.90	18.90
13:00	18.90	18.90	18.90
13:30	18.90	18.90	18.90
14:00	18.70	18.48	18.00
14:30	18.40	17.74	16.30
15:00	17.40	17.24	13.80
15:30	17.40	17.24	11.20
16:00	16.30	14.73	6.00
16:30	15.10	11.96	6.00
17:00	11.20	9.37	6.00
17:30	8.80	7.79	6.00
18:00	6.50	6.32	6.00

Time	Ampere		
	Tracker -2 Axis	Tracker -1 Axis	Static
06:00	45.00	30.30	5.00
06:30	82.00	59.00	18.00
07:00	130.00	99.00	42.00
07:30	168.00	134.90	72.00
08:00	200.00	169.60	110.00

08:30	215.00	191.90	145.00
09:00	225.00	208.80	175.00
09:30	234.00	223.30	200.00
10:00	240.00	233.80	220.00
10:30	246.00	242.70	235.00
11:00	250.00	249.40	248.00
11:30	250.00	250.00	250.00
12:00	250.00	250.00	250.00
12:30	250.00	250.00	250.00
13:00	246.00	242.80	235.00
13:30	238.00	230.20	212.00
14:00	225.00	208.00	170.00
14:30	202.00	177.70	125.00
15:00	180.00	147.70	80.00
15:30	150.00	116.30	48.00
16:00	120.00	87.90	25.00
16:30	85.00	59.80	12.00
17:00	48.00	33.60	7.00
17:30	22.00	15.90	5.00
18:00	5.00	5.00	5.00

Time	Watt		
	Tracker -2 Axis	Tracker -1 Axis	Static
06:00	0.54	0.29	0.03
06:30	1.13	0.69	0.15
07:00	2.05	1.42	0.50
07:30	2.82	2.14	1.01
08:00	3.48	2.88	1.78
08:30	3.78	3.37	2.54
09:00	4.01	3.72	3.12
09:30	4.19	4.00	3.58
10:00	4.37	4.24	3.96
10:30	4.65	4.54	4.30
11:00	4.73	4.68	4.59
11:30	4.73	4.73	4.73
12:00	4.73	4.73	4.73
12:30	4.73	4.73	4.73
13:00	4.65	4.59	4.44
13:30	4.50	4.35	4.01
14:00	4.21	3.84	3.06
14:30	3.72	3.15	2.04
15:00	3.13	2.40	1.10
15:30	2.57	1.76	0.54

16:00	1.97	1.21	0.21
16:30	1.28	0.72	0.07
17:00	0.54	0.31	0.04
17:30	0.19	0.12	0.03
18:00	0.03	0.03	0.03

Based on the test results from 06:00 to 18:00 WIB, the use of the solar tracker is proven to significantly improve solar panel performance compared to a static panel. The two-axis tracker produced the highest output, followed by the one-axis tracker, while the static (fixed) panel gave the lowest performance. In the morning (06:00–09:00) and evening (14:00–18:00), both tracker systems produced far higher voltage, current, and power than the static panel because of their dynamic position following the sun's movement, with the two-axis tracker showing an extra advantage over the one-axis tracker in this period because of its ability to adjust to the still-low solar elevation angle. Conversely, at midday (11:00–13:00) the power difference between the three systems becomes very small and insignificant, because the sun is directly overhead (zenith), so that the horizontally mounted static panel and the one-axis and two-axis tracker panels receive sunlight radiation nearly perpendicularly at almost the same level.

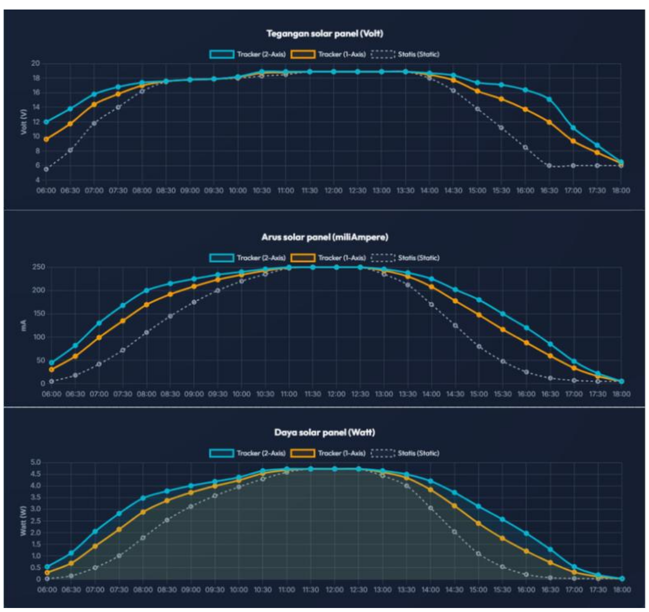

Fig. 18. Comparison of testing between the static panel and the tracker.


Fig. 19. Visualization of solar tracker efficiency over one day.

Overall, the application of this solar tracking system successfully widened the daily energy-production curve substantially, with the two highest power-gain peaks of the tracker system over the static panel occurring at 07:00–08:00 and 15:00–16:00, because the static panel loses much potential power due to the oblique angle of incidence of sunlight at those hours. Based on the energy-accumulation graph, the two-axis tracker system successfully collected a total energy of 38.3 Wh throughout the day, followed by the one-axis tracker system at 34.2 Wh, while the static panel only collected 27.6 Wh. Thus, the application of this solar tracking system is proven to significantly increase solar-energy harvesting efficiency, namely by 38.8% for the two-axis tracker system and 23.9% for the one-axis tracker system compared to the static panel, with the two-axis tracker providing an additional efficiency of 12.0% compared to the one-axis tracker system.

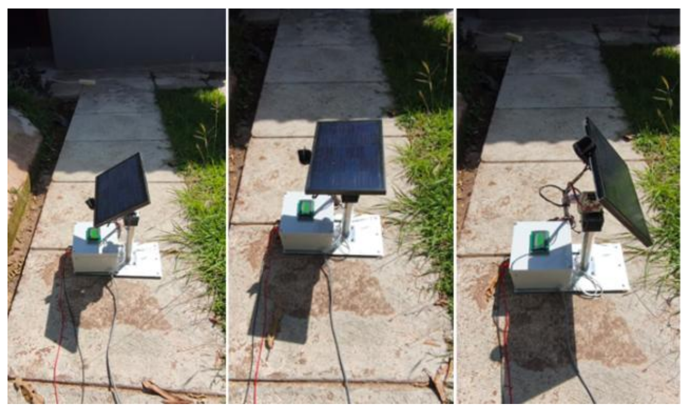
Fig. 20. Overall system testing.

Fig. 20 shows evidence of the tracker's movement in tracking the direction of the sun's heat during the overall system test.

IV. CONCLUSION

Based on the design, testing, and data analysis carried out, it can be concluded that this ESP32 microcontroller-based dual-axis solar tracker system was successfully built and performs quite well: the four-quadrant LDR comparison method proved responsive in directing the solar panel to follow the sun's movement throughout the day, and threshold adjustment successfully reduced the system's "confusion" symptom (the motor moving back and forth while searching for the ideal position), making energy consumption more efficient; IoT integration was also successfully implemented via the ESP32's internal Wi-Fi to send real-time data for remote monitoring of electrical parameters, with the INA3221 sensor proving highly valid compared to a standard digital multimeter, showing a low power error rate; and the solar tracker proved to absorb energy far better than a static panel, with the largest gains occurring in the morning and afternoon when the sun is low—peaking at 07:00–08:00 and 15:00–16:00 WIB—keeping electricity production stable and significantly improving energy absorption efficiency. However, the system still has limitations, namely its dependence on a third-party IoT platform (Blynk) with quota and feature restrictions, a tracking mechanism that relies solely on visible light intensity from the LDR sensor without an alternative heat-direction detection method, and the absence of in-depth mechanical calculations—such as drive motor torque and structural wind resistance—needed for larger-scale implementation in open areas; therefore, future development is recommended to include building an independent IoT server platform instead of relying on Blynk, enhancing the tracking mechanism with sensors capable of detecting the sun's heat direction (not just visible light) to maintain accuracy under thick cloud cover, and scaling up the prototype with deeper mechanical considerations such as motor torque and wind resistance for open-area deployment.

ACKNOWLEDGMENT

The author would like to thank Adlian Jefiza, S.Pd., M.T. and Daniel Sutopo Pamungkas, S.T., M.T., Ph.D. as supervisors for their guidance and knowledge throughout this research, as well as Dr. Abdurahman Dwijotomo, S.ST., M.Sc. and Sulistiono, S.T., M.T. as the examining team.

REFERENCES

[1] S. R. Singh and P. Das, "Performance Analysis of Dual Axis Solar Tracker," *2021 Int. Conf. Comput. Perform. Eval. ComPE 2021*, pp. 273–276, 2021, doi: 10.1109/ComPE53109.2021.9751972.

[2] G. Shukla, A. K. Shukla, K. N. Shukla, and S. Dixit, "IoT-enabled solar PV systems: real-time monitoring and efficiency optimization," *Results Opt.*, vol. 22, no. August 2025, p. 100949, 2026, doi: 10.1016/j.rio.2025.100949.

[3] M. E. S. M. Essa, A. A. Hassan, E. E. El-Kholy, and M. M. R. Ahmed, "Innovations and advancements in solar tracker systems: A comprehensive review," *J. Mechatronics, Electr. Power, Veh. Technol.*, vol. 16, no. 1, pp. 1–14, 2025, doi: 10.55981/j.mev.2025.1004.

[4] D. D. Prasanna Rani, D. Suresh, P. Rao Kapula, C. H. Mohammad Akram, N. Hemalatha, and P. Kumar Soni, "IoT based smart solar energy monitoring systems," *Mater. Today Proc.*, vol. 80, no. xxxx, pp. 3540–3545, 2023, doi: 10.1016/j.matpr.2021.07.293.

[5] R. Xu, X. Ji, C. Liu, J. Hou, Z. Cao, and H. Qian, "Design and Control of a Wave-Driven Solar Tracker," *IEEE Trans. Autom. Sci. Eng.*, vol. 20, no. 2, pp. 1007–1019, 2023, doi: 10.1109/TASE.2022.3177353.

[6] S. S. Hosseini Dehshiri and B. Firoozabadi, "Comparison, evaluation and prioritization of solar photovoltaic tracking systems using multi criteria decision making methods," *Sustain. Energy Technol. Assessments*, vol. 55, no. March 2022, 2023, doi: 10.1016/j.seta.2022.102989.

[7] E. A. M. Babars, S. M. Abdraboo, M. El-Sayed, M. Essa, and S. Y. El-Mashad, "Modelling and Control of an Experimental Fuzzy Logic Controlled Dual-Axis Solar Tracking System based on Field Programmable Gate Array," *Int. Res. J. Eng. Technol.*, pp. 139–147, 2024, [Online]. Available: www.irjet.net

[8] W. A. Jabbar, S. Annathurai, T. A. Tajul, and M. F. Mohd Fauzi, "Smart energy meter based on a long-range wide-area network for a stand-alone photovoltaic system," *Expert Syst. Appl.*, vol. 197, no. May 2021, p. 116703, 2022, doi: 10.1016/j.eswa.2022.116703.

[9] E. R. A. Larico, "Intelligent dual-axis solar tracking system in the Peruvian highlands: Implementation and performance," *Proc. 2021 IEEE Eng. Int. Res. Conf. EIRCON 2021*, pp. 8–11, 2021, doi: 10.1109/EIRCON52903.2021.9613436.

[10] Di. Halder, F. Amsaad, N. Fourty, and B. Hildebrand, "A Low-Power IoT-enabled Smart Monitoring System for Efficient Product Delivery," *Midwest Symp. Circuits Syst.*, vol. 2021-Augus, pp. 692–695, 2021, doi: 10.1109/MWSCAS47672.2021.9531872.

[11] B. Zhao, H. Wang, Z. Huang, and Q. Sun, "Location mapping for constructing biomass power plant using multi-criteria decision-making method," *Sustain. Energy Technol. Assessments*, vol. 49, no. November 2021, p. 101707, 2022, doi: 10.1016/j.seta.2021.101707.

[12] R. M. Elavarasan, S. Leoponraj, J. Vishnupriyan, A. Dheeraj, and G. Gangaram Sundar, "Multi-Criteria Decision Analysis for user satisfaction-induced demand-side load management for an institutional building," *Renew. Energy*, vol. 170, pp. 1396–1426, 2021, doi: 10.1016/j.renene.2021.01.134.

[13] B. H. Hameed and S. Kurnaz, "Secure low-cost photovoltaic monitoring system based on LoRaWAN network and artificial intelligence," *Discov. Comput.*, vol. 27, no. 1, 2024, doi: 10.1007/s10791-024-09475-0.

[14] M. Belik and O. Rubanenko, "Sensitivity analysis of digital twin model for energy community PV system," *Sci. Rep.*, vol. 15, no. 1, pp. 1–24, 2025, doi: 10.1038/s41598-025-13707-8.

[15] X. Zhao, "A novel digital-twin approach based on transformer for photovoltaic power prediction," *Sci. Rep.*, vol. 14, no. 1, pp. 1–17, 2024, doi:

10.1038/s41598-024-76711-4.